An x-ray diffraction and ^{31}P MAS NMR study of rare-earth phosphate glasses, $(R_2O_3)_x(P_2O_5)_{1-x}$, x = 0.175-0.263, R = La, Ce, Pr, Nd, Sm, Eu, Gd, Tb, Dy, Ho, Er

2001 J. Phys.: Condens. Matter 13 4105

(http://iopscience.iop.org/0953-8984/13/18/318)

INSTITUTE OF PHYSICS PUBLISHING JOURNAL OF PHYSICS: CONDENSED MATTER

J. Phys.: Condens. Matter **13** (2001) 4105–4122 www.iop.org/Journals/cm PII: S0953-8984(01)20470-6

An x-ray diffraction and ^{31}P MAS NMR study of rare-earth phosphate glasses, $(R_2O_3)_x(P_2O_5)_{1-x}$, x = 0.175–0.263, R = La, Ce, Pr, Nd, Sm, Eu, Gd, Tb, Dy, Ho, Er

Jacqueline M Cole[1,4], Ernst R H van Eck[1], Gavin Mountjoy[1], Ruth Anderson[1], Tessa Brennan[2], Graham Bushnell-Wye[3], Robert J Newport[1] and George A Saunders[2]

[1] School of Physical Sciences, University of Kent at Canterbury, Canterbury, Kent CT2 7NR, UK
[2] Department of Physics, University of Bath, Claverton Down, Bath BA2 7AY, UK
[3] Synchrotron Radiation Source, Daresbury Laboratory, Daresbury, Warrington, Cheshire WA4 4AD, UK

E-mail: jmc61@cam.ac.uk (J M Cole)

Received 5 January 2001

Abstract

An x-ray diffraction and ^{31}P MAS NMR study of rare-earth phosphate glasses of composition, $(R_2O_3)_xP_2O_5)_{1-x}$, where $x = 0.175$–0.263 and R = La–Er (except for Pm), is presented. The structures of these materials were investigated as a function of (a) rare-earth atomic number and (b) glass composition. The results show an increase in rare-earth coordination number from six to seven as the rare-earth ion increases in size. This effect is most evident for the rare earths, Ce, Pr and Nd, and appears to be independent of composition variation. The implications of sevenfold coordination in these glasses with respect to the possibilities of rare-earth clustering are discussed, as is the role of the incorporation of aluminium impurities in this regard. The increase in levels of cross-linking within the phosphate network, as a consequence of these small amounts of aluminium, is illustrated, as is the changing nature of the phosphate groups as a function of composition. The first reliable and quantitative parametrization of the second and third neighbour R–(O)–P and R–(OP)–O correlations is also given and the stability of the structures to strain when the glasses are drawn as fibres or exposed to different thermal conditions is described.

[4] Author for correspondence. Present address: Department of Chemistry, University of Cambridge, Lensfield Road, Cambridge CB2 1EW, UK

0953-8984/01/184105+18$30.00

1. Introduction

Rare-earth (R) phosphate glasses with stoichiometries close to those of metaphosphate, $R(PO_3)_3$, and ultraphosphate, RP_5O_{14}, species have shown great promise in the laser and optoelectronics industry. This is because the rare-earth ions possess the required energy levels for achieving successful population inversion and the nonlinear refractive index is large enough to exhibit the desired effects without causing beam breakup and damage. Moreover, the particularly high concentration of rare-earth dopant present in these materials incurs a myriad of exotic physical properties at low temperatures: negative thermal expansion (Acet *et al* 1998), negative pressure dependence of bulk moduli (Mierzejewski *et al* 1988) and unprecedented magnetic, magneto-optical and opto-acoustic phenomena (Carini *et al* 1997).

Despite this multitude of exciting properties, their fundamental structural origins are not well understood. The nature of the atomic structure of these glasses evidently plays an important role in their physical characteristics. However, such knowledge is sparse, to the extent that a concerted structural programme is being followed in order to establish a coherent picture of the glass microstructure.

Due to the high structural complexity of glasses, extensive use of a wide range of structural probes is necessary in order to piece together the structure of these materials. Previous work has concentrated on fluorescence (Farok *et al* 1992, Acet *et al* 1998, Brennan *et al* 1999) and Raman spectroscopy (Mierzejewski *et al* 1988, Lipinska-Kalita *et al* 1995), EXAFS (Bowron *et al* 1995, 1996b, Anderson *et al* 1999) and neutron (Hoppe *et al* 1998, Cole *et al* 1999) and x-ray diffraction (Bowron *et al* 1995, 1996a) techniques. The spectroscopic results showed that the rare-earth dopants exist as tripositive ions and are embedded in a phosphate network. EXAFS studies on all of the title compounds confirmed these findings and also yielded average R–O distances of 2.42(1)–2.23(1) Å, decreasing in accordance with the lanthanide contraction. In addition, the EXAFS results showed that the R^{3+} ions are surrounded exclusively by between six and eight oxygen ions, these limits corresponding to the coordination numbers of the ultra- ($x = 0.167$) and meta- ($x = 0.25$) phosphate crystalline analogues (see for example Cole *et al* 2000, Hong 1974). The EXAFS spectra also intimated the existence of a second neighbour R–(O)–P correlation in the vicinity of 3.1–3.6 Å and one third neighbour correlation, R–(OP)–O, in the region of 4.0–4.1 Å.

Complementary neutron diffraction studies (Hoppe *et al* 1998, Cole *et al* 1999) corroborated these EXAFS results and quantified the immediate rare-earth environment more precisely. Correlations due to the phosphate network were located and quantified; in particular, terminal and bridging P–O correlations were resolved well and second (O–(P)–O and P–(O)–P) and third (P–(OP)–O) neighbour separations were located with good accuracy. Aluminium impurities, incorporated within the glass network during sample fabrication, were also detected and their important role in strengthening these glass structures was deduced by ^{27}Al MQMAS NMR investigations.

The relative neutron scattering cross-sections of R, P and O nuclei are such that correlations involving P and O atoms tend to dominate the resulting spectra of the subject compounds. Moreover, high absorption cross-sections and the prevalence of nuclear resonances in the dynamic range of interest are associated with the rare-earth component of these materials, such that only a limited number of rare-earth phosphate glasses can be studied by neutron diffraction. The additional use of x-ray diffraction techniques to study these glasses is therefore highly complementary to the neutron diffraction studies previously reported (Hoppe *et al* 1998, Cole *et al* 1999). The entire range of rare-earth phosphates can be studied by x-ray diffraction, as in the EXAFS studies, and x-ray atomic scattering factors are such that R–X correlations dominate, rather than P–X and O–X correlations as in neutron diffraction.

An x-ray diffraction study of the rare-earth phosphate glasses, $(R_2O_3)_xP_2O_5)_{1-x}$, $x = 0.187$–0.260, R = Ce–Er (except for Pm as it is radioactive) is therefore presented herein. This work builds on initial x-ray diffraction studies on these materials (Bowron *et al* 1995, 1996b) which comprised investigations of $(Pr_2O_3)_{0.216}(P_2O_5)_{0.784}$, $(Eu_2O_3)_{0.252}(P_2O_5)_{0.748}$ and $(Tb_2O_3)_{0.263}(P_2O_5)_{0.737}$. These data have also been incorporated into the present investigation, in combination with the new data, since a more extensive modelling of the data is described.

Given the industrial potential of these materials as optical fibres, x-ray diffraction experiments on selected rare-earth phosphate glasses drawn as fibres were also carried out. A comparison of these structural data with those of the bulk glasses is made and the effects of temperature on the structure of the fibres are also assessed.

The much lower sensitivity of x-ray diffraction towards the phosphate network, compared to neutron diffraction, is complemented here by ^{31}P MAS NMR studies. The omnipresence of paramagnetism within these materials, due to the rare-earth component, yields broad spectra but, nevertheless, quantifiable conclusions regarding the nature of the phosphate matrix can be deduced. Particular attention is given to the effects of the presence of aluminium impurities in the glasses on the nature of the phosphate network.

2. Experiment

2.1. Sample preparation and characterization

All samples, except for $(Nd_2O_3)_{0.175}(P_2O_5)_{0.825}$, $(Nd_2O_3)_{0.181}(P_2O_5)_{0.819}$ and NdP_5O_{14}, were prepared by heating 25 mol% of the high purity (99.9%) grade rare-earth oxide in the presence of excess P_2O_5 in an aluminium oxide crucible at a temperature corresponding to the rare-earth oxide melt (1400–1650 °C); full synthetic details are described by Mierzejewski *et al* (1988). For the glasses, $(Nd_2O_3)_{0.175}(P_2O_5)_{0.825}$ and $(Nd_2O_3)_{0.181}(P_2O_5)_{0.819}$, 25 mol% of high purity (99.9%) grade Nd_2O_3 was heated to 1000 °C in a platinum crucible in the presence of excess P_2O_5. In all cases, the challenging thermal conditions of the synthetic process, to some degree, make it difficult to attain exact compositional precision. However, it is possible to synthesize such materials within the compositional region of meta- and ultraphosphate. The glass fibres were hand drawn from the melt. The rare earth concentrations in the resulting samples were deduced by electron probe microanalysis and their atomic densities were measured by conventional gravimetric analysis. The crystalline NdP_5O_{14} sample was prepared according to the procedure of Danielmeyer *et al* (1974).

2.2. X-ray diffraction experiments

All experiments were carried out on Station 9.1 at the synchrotron radiation source (SRS), Daresbury Laboratory, UK. The finely powdered bulk samples were enclosed inside a 0.5 mm thick circular metal annulus by kapton windows and mounted onto a flat-plate instrumental set-up. The fibres were glued such that they protruded from the end of a syringe needle, which was mounted onto the centre-stick of a helium-flow cryostat. Using a wavelength, $\lambda = 0.49$ Å, data were collected in transmission across the range $2\theta = 2$–125° ($Q = 0.45$–22.7 Å^{-1}) in 0.2° increments using conventional 2θ–ω bisecting geometry. Lorentz and polarization corrections were applied to the resulting data and a background subtraction was performed. Flat-plate or cylindrical (Bond 1959) absorption corrections were made subsequently on the bulk and fibre data respectively. An iterative method was used to scale and fit the experimental data to the sum of the theoretical values for Compton (Cromer and Mann 1967, Cromer 1969) and atomic

scattering (Cromer and Mann 1968) as a function of 2θ. The interference function, $i(Q)$, in atomic units was then deduced using the relationship

$$i(Q) = \frac{I_{\text{exp}} - (\langle f^2 \rangle + I_c)}{\langle f \rangle^2 \bar{z}^2}$$

where $Q = 4\pi(\sin\theta)/\lambda$, I_{exp} is the corrected experimental intensity, I_c is the normalized sum of the relative Compton contributions from each atom type, $\langle f^2 \rangle$ is the sum of the relative contributions of the square of the self-scattering factor from each atom type, $\langle f \rangle^2$ is the sum of the square of the relative contributions of the self scattering factor from each atom type and $\bar{z}$ is the mean number of electrons in a normalized scattering unit.

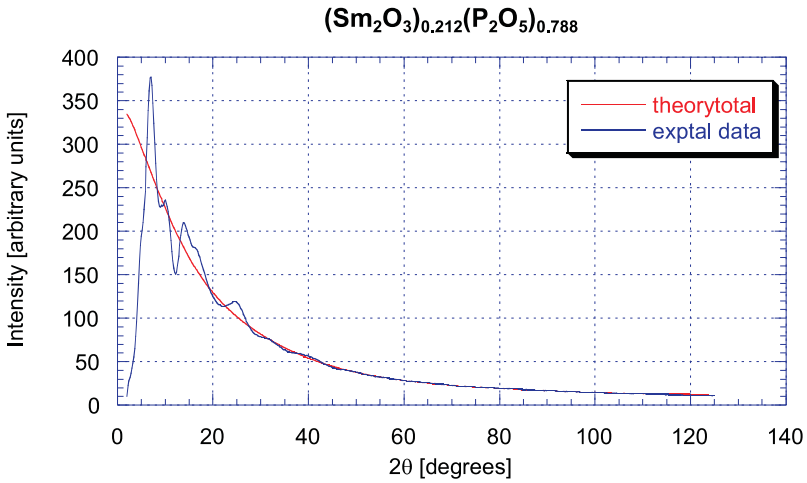

Figure 1. An example of a fit of the corrected experimental data (solid line) to the theoretical sum of self-scattering and Compton contributions (dotted line) as a function of 2θ, using $(Sm_2O_3)_{0.212}(P_2O_5)_{0.788}$ data.

The statistical quality of the data at high angles, and the effects of the cryostat window supports, limited the experiment such that values of Q_{max} of 18.1 Å^{-1} and 12.0 Å^{-1} were obtained for the bulk and fibre data respectively. This implies respective real-space resolutions, $\Delta r \approx 2\pi/Q_{max}$ of 0.35 Å and 0.52 Å.

The atomic pairwise distribution function, $t(r)$, was evaluated by a Fourier transform according to the equation

$$t(r) = 2\pi^2 r\rho_0 + \int_{Q_{min}}^{Q_{max}} Qi(Q)\sin(Qr)\mathrm{d}Q$$

where r is the atomic separation between atoms, and ρ_0 is the atomic density. For the bulk data, atomic pair functions were then simulated in reciprocal space according to the equation (Gaskell 1991)

$$p_{ij}(Q) = N_{ij}(w_{ij}/c_j)(\sin(QR_{ij})/(QR_{ij}))(\exp(-Q^2\sigma_{ij}^2/2)$$

where $p_{ij}(Q)$ is the pair function in reciprocal space, N_{ij}, R_{ij} and σ_{ij} are the coordination number, atomic separation and thermal parameters respectively of atom i with respect to j, c_j is the composition of atom j and w_{ij} is the weighting function of atoms i and j, which follows the relation

$$w_{ij} = (2c_i f_i(Q)c_j f_j(Q))/\overline{f(Q)}^2 \qquad \text{where } i \neq j$$

or

$$w_{ij} = (c_i f_i(Q))^2 / \overline{f(Q)}^2 \qquad \text{where } i = j.$$

Initial estimates of the values of R_{ij}, N_{ij} and σ_{ij} for each pair function were made based on the features present in the experimental $t(r)$ curve, and each pair function was converted into $t(r)$ via a Fourier transform according to the equation

$$t(r) = \int_0^{Q_{max}} Q p_{ij}(Q) \sin(Qr)\, \mathrm{d}Q.$$

The R_{ij}, N_{ij} and σ_{ij} parameters were then refined iteratively and the procedure above repeated until the sum of the Gaussian models best emulated the experimental curve.

2.3. Solid-state ^{31}P *MAS NMR experiments*

All ^{31}P MAS NMR experiments were performed on a CMX infinity 300 solid-state NMR spectrometer at a magnetic field strength of 7.05 T using a 4 mm HX MAS probe, which was resonant at 121.547 MHz for ^{31}P. Chemical shifts were referenced with respect to 85% H_3PO_4 at 0 ppm. All spectra were acquired at a magic angle spinning speed of 15 kHz except for the polycrystalline NdP_5O_{14} where data were collected at both 15 kHz and 16 kHz so that the assignments to each peak could be made unambiguously (given the prevalence of spinning side-bands). Rotor synchronized spin-echo spectra were collected using an RF-field strength of 130 kHz and passive synchronization. Spin–lattice relaxation (T_1) measurements were made at 15 kHz by using a saturation recovery pulse sequence with 40 saturation pulses.

3. Results

The compositions and densities of each $(R_2O_3)_xP_2O_5)_{1-x}$ glass studied are given in table 1. All samples studied by x-ray diffraction also contain small traces (1–2 wt%) of aluminium impurity. An example of a fit of the corrected x-ray diffraction experimental data profile to the curve generated from the sum of the theoretical atomic and Compton scattering as a function of 2θ is given in figure 1. These fits were of good quality, thus indirectly corroborating the accuracy of the chemical composition measurements. The profiles of the $i(Q)$ functions for the bulk and fibre samples, as deduced from the diffraction data, are shown sequentially in figures 2 and 3 respectively. For clarity, the $i(Q)$ functions from previously studied Pr, Eu and Tb bulk samples (Bowron *et al* 1995, 1996b) are also plotted in figure 2. Figure 4 shows both the experimental and modelled $t(r)$ functions for the bulk samples. The experimental $t(r)$ profiles of the Pr, Eu and Tb samples are also taken from the aforementioned previous studies but the modelling of *all* data sets up to 4 Å derives from this work. An illustration of the manner in which individual Gaussian peaks combine to form this total $t(r)$ model is given in figure 5 using the example of $(Sm_2O_3)_{0.212}(P_2O_5)_{0.788}$. A total of seven Gaussian peaks were fitted to the experimental $t(r)$ profile in each case. Table 2 lists the nature of these correlations along with their atomic separation, R, coordination number, N, and Debye–Waller factor, σ^2. The model was applied up to a distance of ∼4 Å, beyond which the preponderance of overlapping correlations precluded any further unambiguous modelling. In the range modelled, the experimental $t(r)$ profile is emulated very well, except in the vicinity of 1.8 Å. This residual feature is known to derive from correlations that pertain to the presence of a small amount of Al contaminant (Cole *et al* 1999) but it cannot be modelled as it is small and broad (since it relates to several different Al–O environments).

The low Q_{max} accessible for the fibre data precluded any quantitative modelling of the correlations present in real space. Nevertheless, direct comparisons of the $i(Q)$ functions of

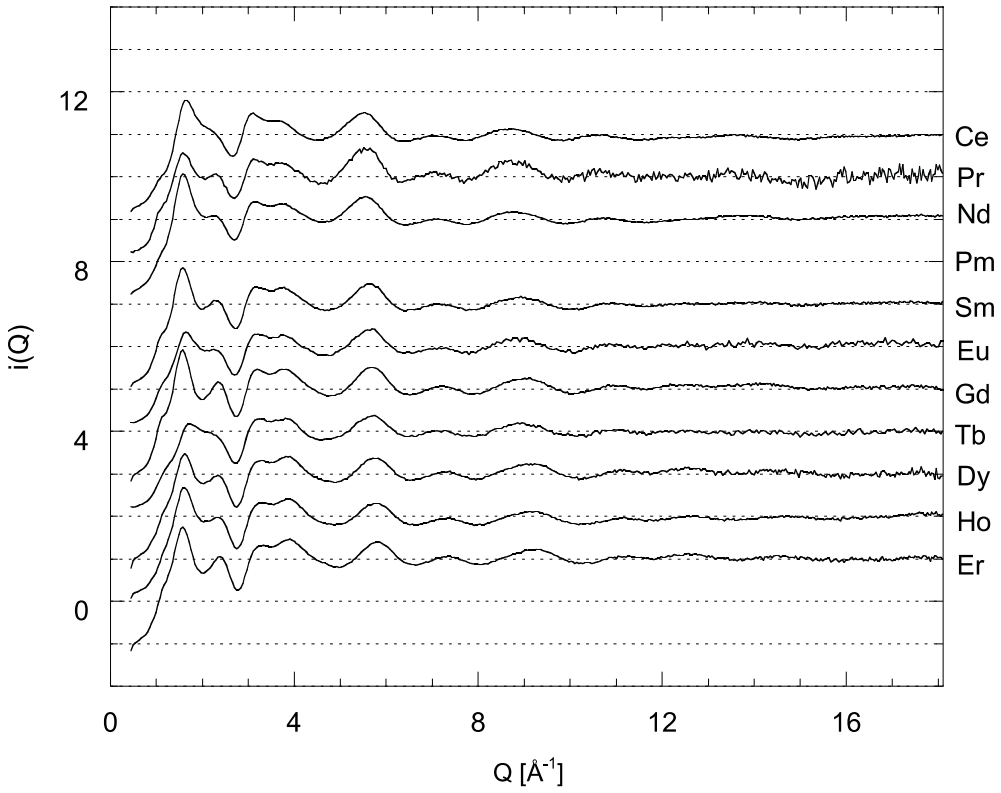

Figure 2. Interference functions, $i(Q)$, for the glasses $(R_2O_3)_xP_2O_5)_{1-x}$, R = Ce–Er (except Pm) $x = 0.187$–0.263, in their bulk form.

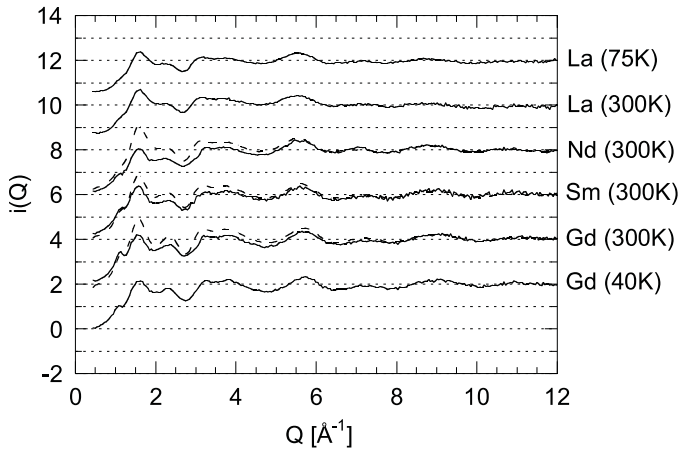

Figure 3. Interference functions, $i(Q)$, for the glasses $(R_2O_3)_xP_2O_5)_{1-x}$, R = La (75 K), La (300 K), Nd (300 K), Sm (300 K), Gd (300 K) and Gd (40 K), $x = 0.192$–0.230, in their fibre form. The dotted lines represent interference functions for the analogous bulk material.

each data set could be made with a view to assessing whether or not any structural differences were present between the fibre and bulk and between fibres at different temperatures. The

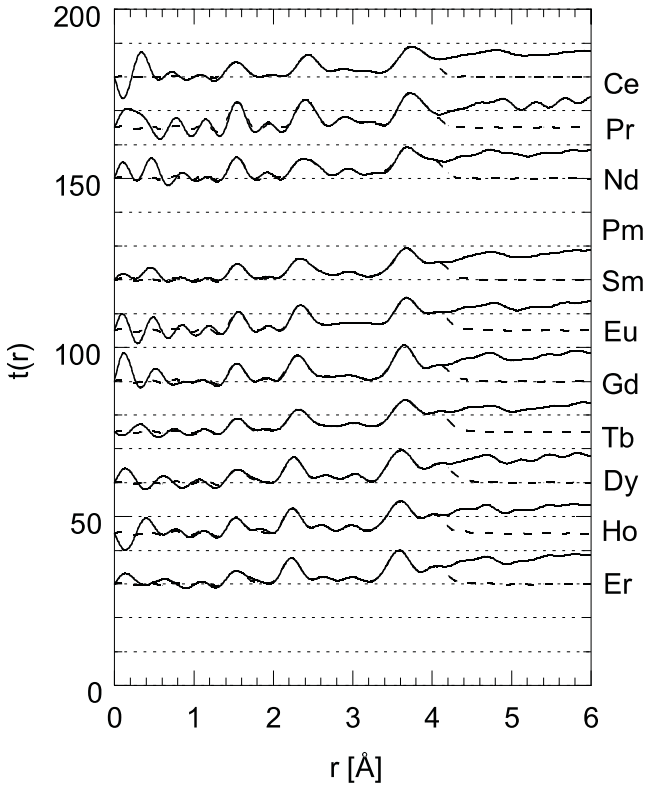

Figure 4. $t(r)$ profiles for $(R_2O_3)_xP_2O_5)_{1-x}$, R = Ce–Er (except Pm); $x = 0.187$–0.263. The solid and dashed lines represent the experimental model and residual to the fit respectively.

Table 1. The compositions and densities of the rare-earth phosphate glasses, $(R_2O_3)_xP_2O_5)_{1-x}$, used in the x-ray diffraction studies. All of these glasses also contain small traces (1–2 wt%) of aluminium.

R	x [±0.005]	ρ (g cm^{-3})	R	x [±0.005]	ρ (g cm^{-3})
	Bulk samples		Dy	0.225	3.37
Ce	0.235	3.12	Ho	0.231	3.52
Pr	0.216	3.09	Er	0.239	3.49
Nd	0.187	3.09		Fibre samples	
Sm	0.212	3.33	La	0.200	3.10
Eu	0.252	3.44	Nd	0.215	3.25
Gd	0.229	3.37	Sm	0.192	3.15
Tb	0.263	3.58	Gd	0.230	3.38

interference features of all fibre data appear to be the same as the corresponding bulk $i(Q)$ profiles within experimental error, and their structures temperature invariant in the range 40–300 K, within the detection limits of the diffraction study. The ostensible disparity between the *underlying* shape of the fibre data and that of the bulk data arises from intrinsic limitations of the fibre data (associated with the fact that they were neither perfectly cylindrical nor of uniform section, which resulted in unreliable Compton, absorption and self-scattering corrections).

Chemical shifts and T_1 relaxation times for all data, as deduced from the ^{31}P MAS NMR measurements, are summarized in table 3. The varying paramagnetic nature of the rare earth

Table 2. Coordination numbers, N, interatomic separations, R, and Debye–Waller factors for each of the seven modelled atomic pairwise correlations modelled using the x-ray diffraction data. The rare-earths marked with an asterisk denote the modelling of data that originated from Bowron *et al* (1995 and 1996b).

Rare			P–O			R–O			O–(P)–O			P–(O)–P		
earth	At. no	Composition	N	R	σ^2	N	R	σ^2	N	R	σ^2	N	R	σ^2
Ce	58	0.235	3.9(3)	1.54(1)	0.005(1)	6.5(6)	2.42(2)	0.009(3)	4.7(9)	2.63(4)	0.005(4)	2.4(1.3)	2.94(4)	0.005(4)
Pr*	59	0.216	5.0(4)	1.55(1)	0.001(1)	6.6(7)	2.38(2)	0.007(3)	5.3(8)	2.53(3)	0.003(3)	2.7(9)	2.93(2)	0.001(2)
Nd	60	0.187	3.8(3)	1.55(1)	0.001(1)	6.4(6)	2.36(2)	0.011(4)	4.7(7)	2.56(2)	0.003(3)	2.5(8)	2.95(2)	0.003(2)
Sm	62	0.212	3.7(3)	1.56(1)	0.003(1)	6.5(6)	2.33(2)	0.010(3)	5.3(8)	2.57(3)	0.004(3)	2.8(9)	2.96(5)	0.006(4)
Eu*	63	0.252	4.4(4)	1.57(1)	0.001(1)	5.6(6)	2.33(2)	0.004(3)	7.3(8)	2.55(3)	0.004(3)	3.0(1.3)	2.96(3)	0.001(2)
Gd	64	0.229	4.0(3)	1.55(1)	0.001(1)	7.1(6)	2.30(2)	0.009(2)	4.7(8)	2.55(3)	0.006(3)	2.7(1.0)	2.95(3)	0.006(3)
Tb*	65	0.263	3.8(3)	1.56(1)	0.002(1)	6.6(6)	2.32(2)	0.011(2)	4.8(8)	2.58(3)	0.002(3)	4.1(1.3)	2.96(4)	0.008(4)
Dy	66	0.225	3.5(4)	1.57(1)	0.003(2)	6.5(5)	2.26(1)	0.008(2)	4.9(7)	2.61(2)	0.006(3)	3.6(1.2)	3.00(3)	0.007(3)
Ho	67	0.231	3.9(3)	1.55(1)	0.001(1)	5.8(5)	2.24(1)	0.006(2)	5.9(7)	2.55(2)	0.005(3)	3.4(1.2)	2.98(3)	0.007(3)
Er	68	0.239	3.9(4)	1.55(1)	0.003(2)	6.6(5)	2.23(1)	0.009(2)	4.9(8)	2.58(2)	0.009(3)	3.4(1.2)	2.97(3)	0.010(3)

Rare			O-(R)-O			R–(O)–P			R–(OP)–O		
earth	At. no	Composition	N	R	σ^2	N	R	σ^2	N	R	σ^2
Ce	58	0.235	7(2)	3.25(5)	0.009(5)	7.6(3.0)	3.70(2)	0.022(6)	12(9)	3.96(6)	0.020(8)
Pr*	59	0.216	8(4)	3.23(4)	0.007(4)	8.9(3.1)	3.71(3)	0.020(5)	11(8)	3.98(6)	0.020(8)
Nd	60	0.187	8(2)	3.27(4)	0.011(5)	8.6(3.0)	3.67(2)	0.020(4)	16(12)	4.00(5)	0.020(7)
Sm	62	0.212	7(3)	3.28(4)	0.010(4)	9.5(2.4)	3.67(1)	0.025(4)	14(11)	4.07(5)	0.021(7)
Eu*	63	0.252	10(6)	3.24(6)	0.005(4)	8.4(2.1)	3.67(1)	0.022(3)	14(10)	4.06(5)	0.021(7)
Gd	64	0.229	5(3)	3.25(5)	0.009(6)	9.7(2.4)	3.64(1)	0.021(3)	13(10)	4.07(5)	0.020(7)
Tb*	65	0.263	9(4)	3.21(5)	0.009(4)	9.7(2.6)	3.65(1)	0.030(3)	14(10)	4.07(6)	0.020(7)
Dy	66	0.225	4(2)	3.19(6)	0.009(5)	9.6(2.4)	3.60(1)	0.025(3)	16(12)	4.08(5)	0.020(7)
Ho	67	0.231	5(3)	3.24(5)	0.008(4)	8.7(2.2)	3.59(1)	0.022(3)	14(11)	4.01(4)	0.020(6)
Er	68	0.239	5(2)	3.19(5)	0.009(5)	8.9(2.2)	3.58(1)	0.021(3)	13(10)	4.03(4)	0.020(7)

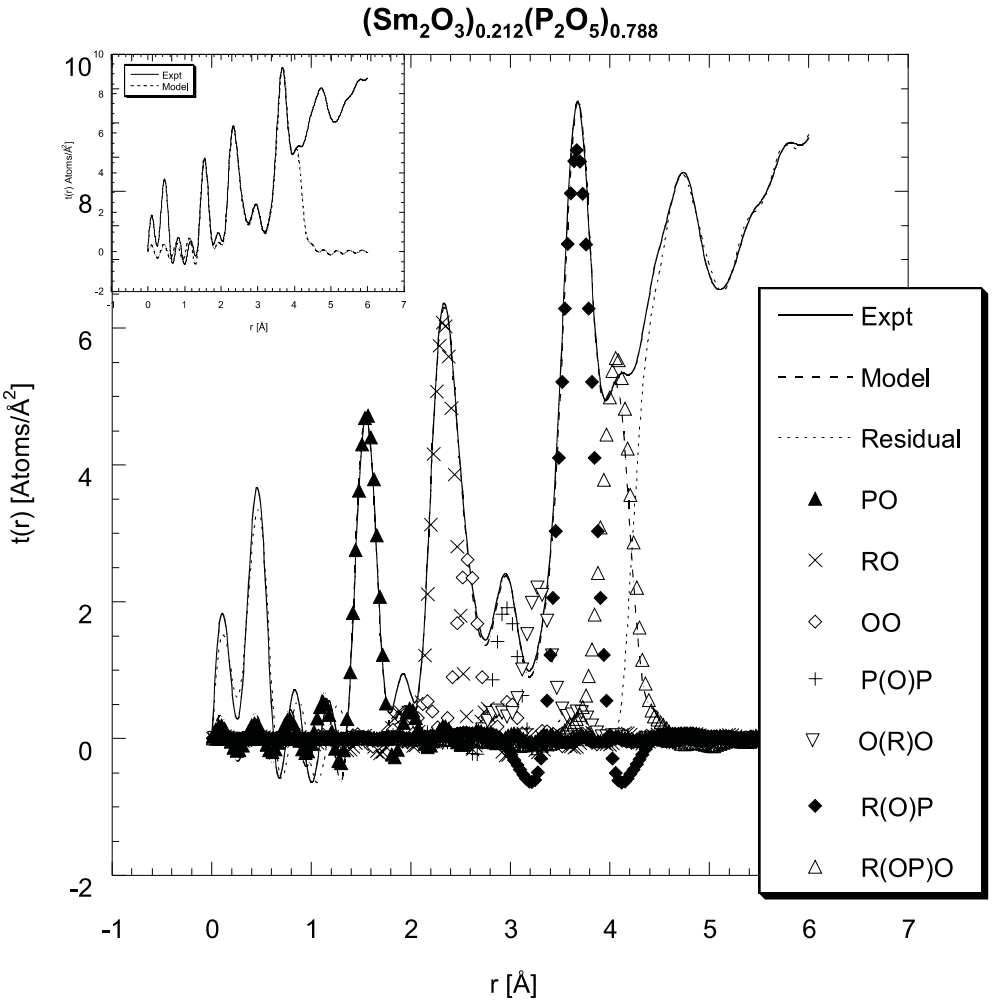

Figure 5. An illustration of the modelling of individual atomic correlations via the example $(Sm_2O_3)_{0.212}(P_2O_5)_{0.788}$. The insert highlights the exceptionally good fit of the total model to the experimental profile. The small discrepancy at ∼1.8 Å is due to the presence of unmodelled Al–O correlations, arising from the small aluminium impurity discussed herein.

in each sample is reflected by the differing widths of the peaks in the spectra. In addition, a significant shift to higher frequency is observed in the neodymium samples that are free from Al contaminant. All neodymium-based ^{31}P NMR spectra are illustrated in figure 6.

4. Discussion

4.1. The immediate rare-earth environment

The decrease in R–O separation with increasing atomic number, R, is representative of the lanthanide contraction, as expected. The values compare well with the analogous neutron diffraction and EXAFS results (see figure 7), the only deviations outside experimental error arising in the data for the larger rare-earth containing glasses: here, the EXAFS values are significantly lower than the diffraction data. However, given the noted problems associated

Table 3. Chemical shifts, peak profiles and T_1 values of rare-earth phosphate glasses with composition $(R_2O_3)_xP_2O_5)_{1-x}$, obtained from ^{31}P MAS NMR results.

$(R_2O_3)_xP_2O_5)_{1-x}$ R	x (±0.005)	T_1 (ms) (±10%)	Chemical shift and peak profile: s = sharp; b = broad; i = intense; w = weak
La	0.225	2.45×10^5	-36bi
Ce	0.197	15	-13bi -150bw
Ce	0.235	10	-6bi
Pr	0.239	89	650 -15bi -600
Pr	0.254	99	700 -4bi -600
Nd	0.187	40	500 70si -4si -38si -400
Nd (no Al)	0.175	(not meas.)	600 43si -22si -500
Nd (no Al)	0.181	(not meas.)	600 45si -20si -500
Nd (no Al)	0.167	34	141si 73si 47si
Sm	0.212	90	-46bi
Sm	0.226	114	-44bi
Eu	0.208	373	500 75sw -39si -236bi -900
Eu	0.218	321	500 84sw -32si -230bi -1000
Gd	0.229	—	TOO BROAD TO MEASURE
Tb	0.263	1.5	2000 ~ -90bi -3000
Dy	0.225	1.2	3000 ~ -150bi -3000
Ho	0.231	1.3	2000 ~ -200bi -2000
Er	0.239	1.7	1500 ~ -250bi -2000

with the presence of double-electron excitations in the EXAFS spectra of these larger rare-earth containing glasses (Anderson *et al* 1999), the diffraction data are expected to reflect the more precise R_{RO} values. Moreover, all EXAFS R_{RO} values are also consistently ∼0.02 Å smaller than the diffraction values and this has been attributed to the assumption of a Gaussian distribution for the ith shell of neighbouring atoms as is common in EXAFS analysis: in reality, this distribution is slightly asymmetric and so this disparity may arise from the systematic neglect of the corresponding $(2\sigma_2/R_i)(1 + R_i/\lambda)$ correction term (Crozier 1997). Bearing these factors in mind, and using tabulated values of ionic radii from Shannon (1976), a clear trend from six- to seven-fold coordinated R^{3+} ions with decreasing rare-earth atomic number is evident. Such a trend was postulated in the previous neutron diffraction studies (Cole *et al* 1999). Moreover, the derivation of O–R–O angles, using the R_{ORO} parameters in addition to the R_{RO} separations, corroborates this trend: an increasing deviation of the O–R–O angle from 90° (octahedral) to an acute angle (>six-coordinate) is evident (see table 4). The coordination numbers, N_{RO}, deduced from this work are also in agreement with this trend within experimental error, although the substantial overlap of the RO atomic pairwise correlations with those of OPO render all derived N_{RO} parameters with very limited accuracy. Such accuracy is particularly poor in the cases associated with the larger rare-earth ions, where such overlap is most severe due to the increasingly similar RO and O–(P)–O separations; thus, the lack of any observable trend of N_{RO} with atomic number, R, is not surprising.

4.2. Implications of a seven-coordinate R^{3+} *environment*

The coordination number of R^{3+} ions appears to increase with ionic size irrespective of the exact composition of the glass. This is very pertinent since it indicates that the rare-earth coordination is dictated by purely geometrical constraints local to the rare-earth ion, rather than being a consequence of the nature of the phosphate network. A seven-coordinate rare-earth

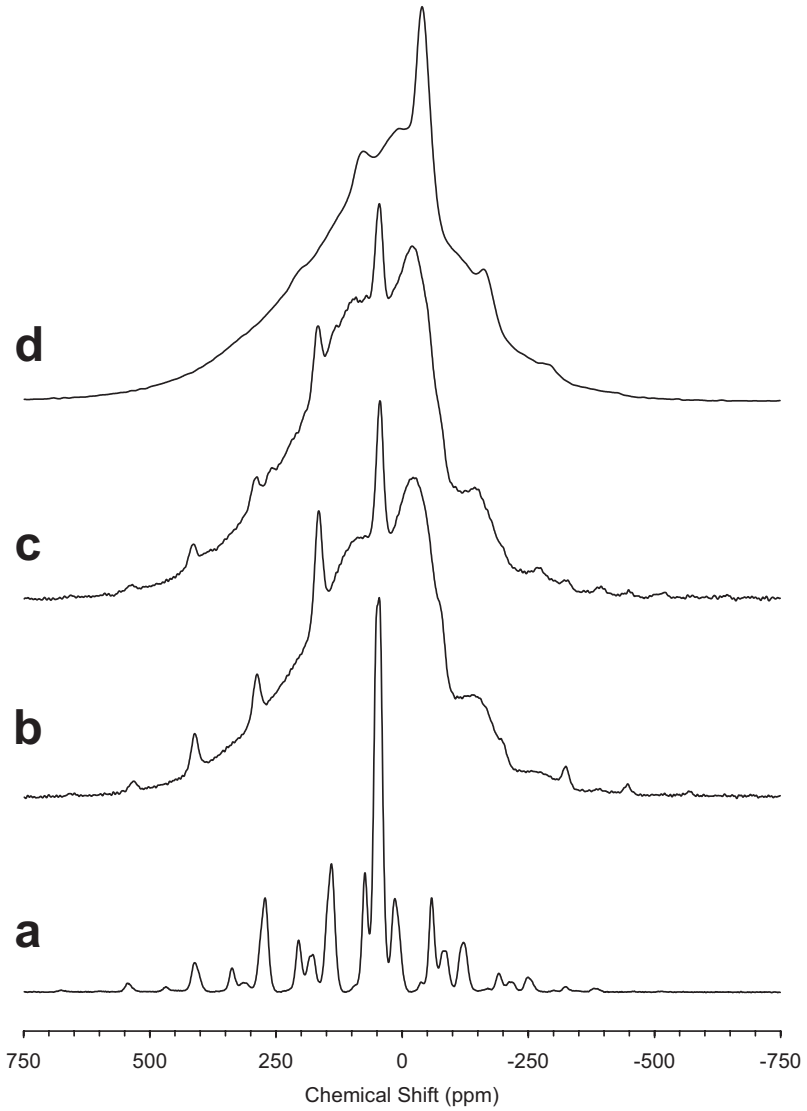

Figure 6. ^{31}P MAS NMR spectra of (a) crystalline NdP_5O_{14} (Al free) (parent peaks for Q^3 lie at 40 ppm and those for Q^2 at 141 and 70 ppm); (b) $(Nd_2O_3)_{0.175}(P_2O_5)_{0.825}$ (Al free); (c) $(Nd_2O_3)_{0.181}(P_2O_5)_{0.819}$ (Al free) and (d) $(Nd_2O_3)_{0.187}(P_2O_5)_{0.813}$ (contains 1–2 wt% Al).

environment has notable implications with respect to the possibility of rare-earth clustering in these glasses; that is to say, in terms of a distance between neighbouring pairs of R^{3+} ions which is shorter than would be the case for a purely statistical distribution based on number density calculations alone. The following argument addresses the matter.

We note the fact that there may be several possible distributions of Q^n species (where Q^n is the number of bridging oxygen bonds associated with a phosphate group: see figure 8) which all maintain overall charge neutrality given the charge-sharing present in modified network glasses, and that the coordination number (which is what is available from diffraction studies) does not in itself constrain the Q^n distribution. However, although we are unable to

Table 4. The variation in O–R–O angle with increasing atomic number, R, in rare-earth phosphate glasses of composition $(R_2O_3)_xP_2O_5)_{1-x}$, as deduced from x-ray diffraction results.

R	O–R–O angle (°)
Ce	84(1)
Pr	86(1)
Nd	88(1)
Sm	90(1)
Eu	88(1)
Gd	90(1)
Tb	88(1)
Dy	90(1)
Ho	93(1)
Er	91(1)

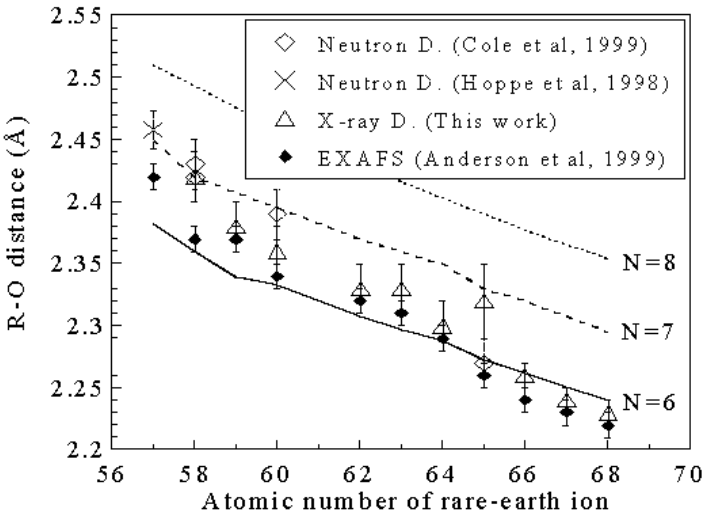

Figure 7. The variation in the R–O distance as a function of rare-earth atomic number, R, according to neutron diffraction (Cole *et al* 1999, Hoppe *et al* 1998), x-ray diffraction (this work) and EXAFS (Anderson *et al* 1999) studies. The dashed lines represent the variation in R–O distance with R calculated using values of ionic radii from Shannon (1976).

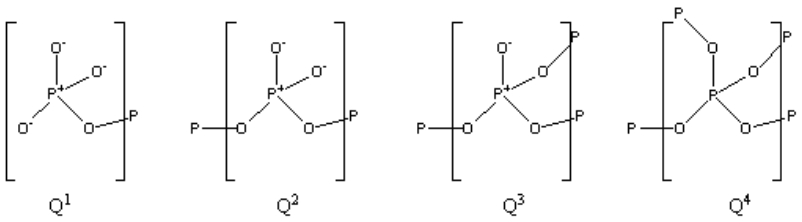

Figure 8. An illustration of the possible different Q^n phosphate group types.

address such issues definitively it is perhaps instructive to consider what are possible structural conformations. PO_4 tetrahedra in the phosphate network of rare-earth metaphosphate crystal structures are all Q^2 species; for glasses with composition close to that of metaphosphate, the stoichiometry dictates that (a) one-third of the oxygens must be bridging and two-thirds

non-bridging or (b) if a mixture of Q^n species is present, then it has an average of Q^2, i.e. any Q^1 and Q^3 species are balanced. However, given a rare-earth coordination greater than six, scenario (a) can only be achieved if one of the R–O oxygens is terminal to two different R^{3+} ions. Such a restriction implies the presence of rare-earth clustering. For scenario (b) to be realized, the oxygens in Q^1 species must be either triply terminal to an R^{3+} ion or terminal to two or three different R^{3+} ions. A phosphate group with oxygens triply terminal to one R^{3+} ion would impose severe geometrical constraints upon a PO_4 tetrahedron—the alternative involvement of several R^{3+} ions is thus the only reasonable model if scenario (b) pertains.

Given the veracity of this argument, the presence of rare-earth clustering in vitreous $La(PO_3)_3$, as conjectured by Hoppe *et al* (1998) would certainly be true. However, in their neutron diffraction study, no corresponding R–(O)–R correlation was detected (although no atomic pairwise correlations beyond ∼3 Å were modelled and the relative weightings of the neutron atomic cross-sections are not favourable for the detection of such a correlation). The data from the present study also fail unambiguously to reveal any R–(O)–R correlations, despite the more favourable atomic scattering factors of R. In this case, many overlapping correlations precluded modelling of the data beyond ∼4 Å, a distance still lower than that expected for an R–(O)–R separation. Admittedly, the glasses presented here predominantly have compositions less than $x = 0.25$, and the closer they become to the ultraphosphate limit, $x = 0.167$, the lower is the requirement for an overall Q^2 phosphate network on average, since the ultraphosphate crystal, RP_5O_{14}, satisfies its stoichiometry by possessing a phosphate network comprising a mixture of Q^2 and Q^3 species. However, given the argument above, the presence of an R–(O)–R correlation for at least the cerium sample reported here ($x = 0.235$) would still be suspected. Moreover, our neutron studies indicate the retention of predominantly Q^2 phosphate network on average (via the presence of a ∼1:1 ratio of $PO_{Terminal}$:$PO_{Bridging}$ bonds) in compounds ranging from $x = 0.26$ to 0.197. The possibility of rare-earth clustering in any of these glasses cannot therefore be ruled out and given that such clustering can severely affect the magnetic and optical properties of these materials, the existence or otherwise of any rare-earth clustering is important to ascertain as, thence, the physical properties of these glasses may be optimized. As a consequence, a related programme involving complementary anomalous scattering techniques and the development of a novel magnetic difference experiment is currently underway to determine conclusively the closest R . . . R atomic separation in these glasses.

4.3. Effects of sample fabrication processes: consequences of Al incorporation

The identification of the presence or lack of rare-earth clustering is also further complicated in this work compared to that of Hoppe *et al* (1998), since the use of an Al_2O_3 crucible in the synthesis of our glasses has been found to result in the additional incorporation of a small trace (∼1–2 wt%) of Al^{3+} ions (Cole *et al* 1999). Indeed, this impurity is responsible for the small broad residual feature present in the $t(r)$ profiles at 1.7–1.9 Å (see figure 4), the broadness being caused by the presence of up to three distinct Al^{3+} structural environments. This contaminant strengthens the glass markedly: the synthesis of an analogous glass in a platinum crucible (i.e. Al free conditions) resulting in a much more brittle and fragile material. A corollary to this increased strength is that a substantial level of phosphate cross-linking must be caused by the presence of Al^{3+} ions, i.e. Al^{3+} ions must induce Q^3 species. It is quite likely that this increasing level of Q^3 species due to the presence of Al^{3+} ions may be complemented by a corresponding increasing presence of Q^1 species. This is because of the common ionic charge of the Al^{3+} and R^{3+} ions, but much smaller ionic size of Al^{3+}: thus, rare-earth clustering that might otherwise occur will therefore be avoided by the alternative formation of R–(O)–Al

interactions, and such an environment has previously been observed via ^{27}Al NMR studies (Cole *et al* 1999).

^{31}P NMR studies on Al-free and Al-containing neodymium phosphate glasses were conducted as part of the present work in order to explore further the influence of Al on the phosphate network. The shift to higher frequencies of peaks in the Al-free samples compared to that of $(Nd_2O_3)_{0.187}(P_2O_5)_{0.813}$ is indicative of the presence of Al. The NdP_5O_{14} sample was used to assign unambiguously the peaks due to Q^2 and Q^3 species, since the crystal structure contains a combination of these phosphate groups in a ratio of 3:2 respectively (Hong 1974). All five phosphorus atoms in the NdP_5O_{14} structure are in fact crystallographically unique and three of these five environments can be resolved distinctly in the ^{31}P NMR spectra: the Q^2 and Q^3 environments are sufficiently different to be resolved, and the bond-lengths of one of the crystallographically unique Q^2 phosphate groups are sufficiently disparate to the other two Q^2 species that this environment can also be isolated[1].

An overall ^{31}P NMR peak integration of 1:2:2 is thus obtained, relating to parent peaks at chemical shifts of 73.6 ppm and 141.1 ppm for Q^2 and 47.1 ppm for Q^3 respectively at a spinning speed of 15 kHz. These three environments were differentiated from each other and from all associated side-bands by comparing rotor synchronized spin-echo spectra recorded at spinning speeds of both 15 and 16 kHz.

The peaks corresponding to Q^3 are naturally sharper than those for Q^2 on account of the lower degree of coupling of the phosphorus to the paramagnetic rare-earth ion. This effect is most evident in the spectra of the glasses due to their highly disordered nature. In fact, whilst a Q^2 phosphate environment is expected to dominate in these materials, any other Q^n phosphate type may also be present to a certain degree. That said, the presence of any Q^0 or Q^4 species is unlikely since their presence is not detected by ^{31}P NMR: such a technique should be particularly sensitive to these environments since their intensities and narrow nature would not be compromised by any coupling to the paramagnetic R^{3+} ions. Moreover, such peaks would also exist at chemical shifts distinctly different to any contributions from other Q^n species. On the other hand, the detection of any Q^1 species is difficult since any peaks associated with this will be heavily broadened by a substantial level of coupling to R^{3+} ions and so, if present, such contributions are expected to lie within the broad envelope generated by the dominant Q^2 contributions. Q^3 species, however, may be distinguished from these broad Q^2 features as their peaks are significant narrower and thus any significant level of Q^3 species will result in the resolution of sharp features at a chemical shift similar to that found in the NdP_5O_{14} crystalline spectrum. The additional detection of spinning side-bands associated with Q^3 species helps confirm the correct assignment of any such parent peaks.

Bearing this in mind, an inspection of the spectra of the neodymium glasses (figure 6) shows that both Q^2 and Q^3 species are present in each case with Q^2 being, by far, the most dominant. The Al-free glasses appear to possess lower amounts of Q^3, relative to Q^2, compared to the Al-containing sample, which has the same composition within experimental error. This corroborates the earlier conjecture that Al aids significantly the level of cross-linking in these glasses.

4.4. The phosphate network

A comparison of the two Al-free neodymium glass spectra also shows notable differences in the relative ratios of Q^2:Q^3 environments present. Given that these two glasses have very similar compositions, this suggests that the nature of the phosphate network is very sensitive

[1] ^{31}P NMR is particularly sensitive to the subtle crystallographic differences in Q^2 species in this sample owing to its paramagnetic nature: even slight changes in orbital overlaps (i.e. by change in angle or distance) reflect strongly in the NMR spectra of ^{31}P.

to composition, at least in the region close to the ultraphosphate limit.

A similar comparison of ^{31}P NMR data from europium glasses with close compositions, $x = 0.208$ and $x = 0.218$, shows that this sensitivity extends to stoichiometries tending more towards the metaphosphate limit. Here, the sharp peaks, due to the presence of Q^3 species, appear at -39 and -32 ppm respectively.

Whilst the high levels of paramagnetism in all other samples preclude the resolution of such peaks from the broader and more dominant Q^2 contributions, the relative centres of their peaks as a function of composition, for samples containing a given rare earth, show a consistent trend of increasingly negative chemical shifts with decreasing rare-earth content. Bearing in mind the relative chemical shifts of assigned Q^2 and Q^3 species from the NdP_5O_{14} crystalline compound, such a trend indicates the increasing presence of Q^3 species with decreasing composition. A similar trend has been observed in ^{31}P NMR studies of sodium phosphate glasses (Brow *et al* 1990). The general conclusion that the phosphate network is very sensitive to composition throughout the meta- to ultraphosphate range, with the steady increase in the level of Q^3 species with decreasing rare-earth content, can therefore be drawn. This is accordance with expectations but corresponds to the first evidence of this situation in these glasses, since analogous diffraction and rare-earth absorption edge EXAFS results lack sensitivity towards the relative Q^n phosphate network constitution.

That said, corresponding x-ray diffraction data corroborate the dominance of Q^2 species via the average values obtained for R_{PO}: all such values are similar to each other and result in a mean P–O separation of 1.55 Å. This distance represents an approximate 1:1 overall ratio of $PO_{Bridging}$:$PO_{Terminal}$ atomic separations, as judged by comparing this mean value with the resolved $PO_{Bridging}$ and $PO_{Terminal}$ distances from complementary neutron data (Cole *et al* 1999, Hoppe *et al* 1998).

The coordination number, N_{PO}, is four within experimental error except in the cases of Pr and Dy, the apparent deviation here probably resulting from the relatively severe Fourier series termination ripples in the low r region and up to the P–O distance. The good overall fit to this coordination number is important since it is known *a priori* to equal 4 and thus serves as a good marker for assessing the reliability of the x-ray diffraction data and the fitting process of all other atomic pairwise correlations.

Beyond the isolated P–O correlation, the x-ray diffraction derived R_{POP} and R_{OPO} parameters are also obtainable and are found to be all similar to each other and reliable as they correspond well to the more accurate neutron derived values, these correlations being more evident using the latter probe. By combining the overall mean R_{POP} value (2.96 Å) with that of R_{PO}, a mean P–O–P angle of 144.3° is obtained. This value is typical for such a structural unit in a regular phosphate network. Associated coordination numbers, N_{POP} and N_{OPO}, are notably higher than one would expect in the x-ray diffraction results on account of the severe overlap with other atomic pairwise distributions. Thus, little credence can be ascribed to the actual values of these parameters, although the consistent trend of high values is an important observation since it indicates that a more diffuse envelope of unmodelled correlations probably lies under these features. Indeed, such additional structure was revealed in our complementary neutron diffraction studies and was assigned to P–(OP)–O atomic pairwise correlations.

The thermal parameters of the correlations, corresponding exclusively to P and O atoms, show that the phosphate network is very rigid and its short-range order is fairly regular, out to the first few neighbours. This observed rigidity is, again, reminiscent of the high levels of cross-linking in our conceptual model of the structure of these glasses.

4.5. Second and third neighbour R–X correlations

The presence of R–(O)–P and R–(OP)–O correlations, as intimated by previous EXAFS studies (Anderson *et al* 1999) is confirmed by this work. The x-ray diffraction derived R_{ROP} values are, however, significantly more reliable and accurate than the values proposed by EXAFS studies alone. This is not surprising since this correlation is weak in the EXAFS signal due to the more diffuse, but far more numerous $R \ldots O$ structural contributions. Moreover, the values obtained from EXAFS are on average 0.35 Å lower than those from diffraction. Multiple scattering effects are likely to be the major cause of this discrepancy since the 'triangular' multiple scattering route R–O–O–R covers a distance of 3.1–3.4 Å, thereby obscuring the true position of any R–(O)–P correlation. The R_{ROP} values obtained from diffraction thus represent the first reliable source of closest $R \ldots P$ separation in these materials. Aside from the magnitude of the associated errors, the reliability of the R_{ROP} values can be further inferred by analysing the difference, $R_{ROP} - R_{RO}$, which should give a constant since R_{PO} does not vary with atomic number, R. The average variance from this constant is indeed small (standard deviation = 0.02). The R_{POR} values also exemplify the lanthanide contraction as expected. The coordination number, N_{ROP}, is notably higher than one would expect due to the underlying trails of Gaussian peaks in this region related to the impending onset of a number of overlapping correlations. Modelling of the R–(OP)–O correlation is, of course, more severely affected by such underlying correlations on account of its larger atomic separation. As a result, coordination numbers and Debye–Waller factors are not reliable, but the favourable atomic scattering factors of R allow one to distinguish the R_{ROPO} parameter fairly reliably, such values comparing well to those derived from the EXAFS study.

4.6. The structural integrity of the glasses when drawn as fibres

Since the physical properties of these glasses have prompted their current testing for possible application as optical fibres, it was deemed pertinent to assess whether or not any structural differences were apparent (i) between the bulk and fibre samples, (ii) between the different fibres and (iii) due to thermal effects. The low real-space resolution of the data obtained from these fibres ($Q_{max} = 12$ Å^{-1}) precluded any definitive modelling of atomic correlations in real space. However, a comparative study was performed by assessing any differences between the relevant profiles of the $i(Q)$ functions.

Figures 2 and 3 show that the bulk data compare well with the fibre data except at low values of Q. The discrepancy at low Q may be indicative of a long-range structural difference, but the differences observed are too small to provide any conclusive evidence. In addition, the rather more severe requirements associated with sample alignment in this case, especially given the fact that these hand-drawn fibres are not perfectly cylindrical, may lead to additional errors at lower scattering angles. Figure 3 also shows that there are no observable differences between each fibre. Similarly, the La and Gd samples are temperature invariant within the detection limits of this diffraction study.

These results are important industrially since they indicate that the strain imposed by the drawing of the fibre does not affect the structure and that the materials are also stable against temperature variation, within the reliability of the method.

5. Conclusions

The x-ray diffraction study reveals seven atomic correlations, four of which relate to the rare-earth environment whilst the other three pertain to the phosphate network. Parameters relating

to the immediate rare-earth environment correspond well to complementary neutron and EXAFS results and comparing these all together, a clear trend of increasing R^{3+} coordination number from six to seven with increasing ionic size emerges. Rare-earth clustering must occur in those glasses with compositions close to the metaphosphate limit *and* R^{3+} coordination numbers approaching seven on average. Such clustering may also be present in glasses with other stoichiometries intermediate between meta- and ultraphosphate. The presence of small amounts of aluminium impurity in these glasses may help avert such rare-earth clustering via the alternative formation of R–(O)–Al interactions. ^{31}P NMR data show that the presence of Al^{3+} ions also induces a substantial level of cross-linking in these materials. The NMR results illustrate well the high sensitivity of the Q^n phosphate group type to composition, and whilst a preponderance of Q^2 species is apparent in the glasses throughout the ultra- to metaphosphate range, a steadily increasing concentration of Q^3 species, as a function of decreasing composition, x, in this range is observed.

Modelling of second and third neighbour R–X correlations up to ∼4 Å was possible using the x-ray diffraction data. This radial limit encompassed R–(O)–P and R–(OP)–O correlations, which, for the first time, could be parametrized in a reliable and quantitative manner.

The possibility of any structural perturbations occurring in these glasses as they are drawn into fibres was also investigated as were the thermal effects on the structures of these fibres, through the temperature range 40–300 K. Within the detection limits of the diffraction study, no differences between the structure of bulk and fibre data, between fibre data, or between fibre data at different temperatures, were observed. The structural integrity of the glasses therefore appears to be maintained through the imposition of strain and temperature variation.

Acknowledgments

The authors wish to thank Ray Jones at the Materials Science Laboratory, SRS, Daresbury, UK, for the use of platinum crucibles and furnaces, Richard Martin from the Department of Physics, University of Bath, for the compositional analysis of the Al free samples, Daniel Bowron for providing the data on Pr, Eu and Tb phosphate glasses and the EPSRC (JMC and TB) for funding.

References

Acet M, Brennan T, Cankurtaran M, Saunders G A and Zähres H 1998 *Phil. Mag.* B **77** 1633

Anderson R, Brennan T, Cole J M, Mountjoy G, Pickup D M, Newport R J and Saunders G A 1999 *J. Mater. Res.* **14** 4706

Bond W L 1959 *International Tables for X-ray Crystallography* vol II ed J S Kasper and K Lonsdale (Birmingham: Kynoch) pp 291–306

Bowron D T, Bushnell-Wye G, Newport R J, Rainford B D and Saunders G A 1996a *J. Phys.: Condens. Matter* **8** 3337

Bowron D T, Newport R J, Rainford B D, Saunders G A and Senin H B 1995 *Phys. Rev.* B **51** 5739

Bowron D T, Saunders G A, Newport R J, Rainford B D and Senin H B 1996b *Phys. Rev.* B **53** 5268

Brennan T, Knight J K and Saunders G A 1999 *Phys. Chem. Glasses* **40** 111

Brow R K, Kirkpatrick R J and Turner G L 1990 *J. Non-Cryst. Solids* **116** 39

Carini G, D'Angelo G, Tripodo G, Fontana A, Rossi F and Saunders G A 1997 *Europhys. Lett.* **40** 435

Cole J M, Lees M R, Howard J A K, Newport R J, Saunders G A and Schoenherr E 2000 *J. Solid State Chem.* **150** 377

Cole J M, van Eck E R H, Mountjoy G, Newport R J, Brennan T and Saunders G A 1999 *J. Phys.: Condens. Matter* **11** 9165

Cromer D T 1969 *J. Chem. Phys.* **50** 4857

Cromer D T and Mann J B 1967 *J. Chem. Phys.* **47** 1892

——1968 *Acta Crystallogr.* A **24** 321

Crozier E D 1997 *Nucl. Instrum. Methods Phys. Res.* B **133** 134

Danielmeyer H G, Jeser J P, Schoenherr E and Stetter W 1974 *J. Cryst. Growth* **22** 298
Farok H M, Saunders G A, Poon W and Vass H 1992 *J. Non-Cryst. Solids* **142** 175
Gaskell P H 1991 *Materials Science and Technology Volume 9: Glasses and Amorphous Materials* ed J Zrzycky (Weinheim: VCH) ch 4
Hong H Y-P 1974 *Acta Crystallogr.* B **30** 468
Hoppe U, Kranold R, Stachel D, Barz A and Hannon A C 1998 *J. Non-Cryst. Solids* **232–234** 44
Lipinska-Kalita K E, Fontana A, Leonardi A, Carini G, D'Angelo G, Tripodo G and Saunders G A 1995 *Phil. Mag.* **71** 571
Mierzejewski A, Saunders G A, Sidek H A A and Bridge B 1988 *J. Non-Cryst. Solids* **104** 323
Shannon R D 1976 *Acta Crystallogr.* A **32** 751